

Activation of Low-Valent, Multiply M–M Bonded Group VI Dimers toward Catalytic Olefin Metathesis via Surface Organometallic Chemistry

Alon Chapovetsky, Ryan R. Langeslay, Gokhan Celik, Frédéric A. Perras, Marek Pruski, Magali S. Ferrandon, Evan C. Wegener, Hacksung Kim, Fulya Dogan, Jianguo Wen, Navneet Khetrpal, Prachi Sharma, Jacob White, A. Jeremy Kropf, Alfred P. Sattelberger,* David M. Kaphan,* and Massimiliano Delferro*



Cite This: <https://dx.doi.org/10.1021/acs.organomet.9b00787>



Read Online

ACCESS |



Metrics & More

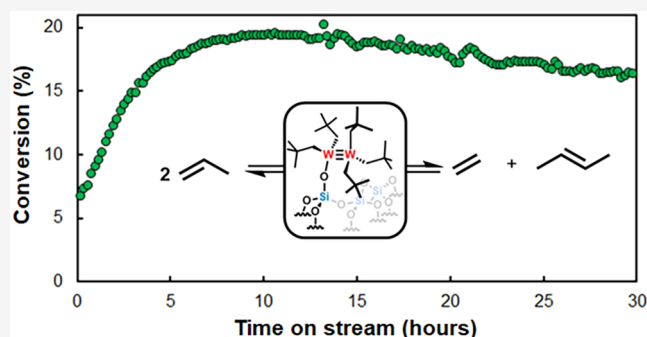


Article Recommendations



Supporting Information

ABSTRACT: Olefin metathesis is a broadly employed reaction with applications that range from fine chemicals to materials and petrochemicals. The design and investigation of olefin metathesis catalysts have been ongoing for over half a century, with advancements made in terms of activity, stability, and selectivity. Immobilization of organometallic complexes onto solid supports such as silica or alumina is a promising strategy for catalyst heterogenization, often resulting in increased activity and stability. Consequently, a broad range of early transition metal catalysts bearing alkyl, oxide/alkoxide, and amide ligands have been grafted onto silica and their reactivities investigated. Herein, we report a series of silica-supported tungsten and molybdenum dimers ($X_3M\equiv MX_3$, where $M = W$ and Mo ; $X =$ neopentyl, tert-butoxide, and dimethyl amide) and their reactivities toward catalytic olefin metathesis. Dynamic nuclear polarization (DNP)-enhanced solid-state nuclear magnetic resonance (SSNMR), diffuse reflectance infrared Fourier transform (DRIFT), UV resonance Raman, and X-ray absorption (XAS) spectroscopies suggest that upon heterogenization the dimers bind to the surface in a monopodal fashion, with the $M\equiv M$ triple bond remaining intact. These structural assignments were further corroborated by density functional theory (DFT) calculations. While the homogeneous dimer counterparts are inert, the supported low-valent alkyl W and Mo dimers become active for the disproportionative self-metathesis of propylene to ethylene and butenes and 4-nonene to 4-octene and 5-decene under mild conditions. The lack of activity observed for the free and supported *tert*-butoxide and dimethyl amide dimers likely suggests that the neopentyl groups are necessary for the formation of a putative alkylidene active species. The difference in reactivity between the free and supported dimers could be explained either by the lowering of the activation barrier of the complex through the electronic effects of the surface or by site isolation of catalytically relevant reactive intermediates.



INTRODUCTION

Olefin metathesis is one of the most widespread reactions performed in the chemical industry with applications ranging from production of fine chemicals to materials and petrochemical processing.^{1,2} For example, propylene, globally the second most extensively produced chemical by volume, is the metathesis product of ethylene and 2-butene.^{3,4} Industrially, propylene production is accomplished using heterogeneous catalysts due to their robust stability, recyclability, and lower separation costs.⁵ However, homogeneous catalyst systems offer significant advantages over their heterogeneous counterparts. Their well-defined structures allow for detailed mechanistic studies and rapid design iteration toward performance optimization. The incorporation of molecular catalyst motifs onto solid supports such as silica, alumina, or zirconia is an

attractive strategy for exploiting these features while benefiting from the increases in stability, activity, and physical characteristics afforded by the heterogeneous support.^{6–15} As such, there has been a major push in recent years to investigate the mechanisms and activities of well-studied organometallic catalysts on silica.^{16–24} The catalytic performance of molecular precursors often serves as a guideline for their selection for heterogenization. Hence, there are a number of studies highlighting the activity of supported early transition metal

Special Issue: Organometallic Chemistry at Various Length Scales

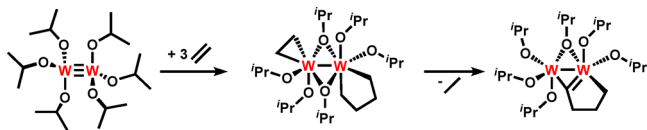
Received: November 18, 2019



complexes bearing ancillary alkyl, oxide, and amide ligands supported on silica.^{25–31} These include but are not limited to alkylidene,^{27,32} imido-alkylidene,^{33,34} thiolate,^{26,35} oxo,^{27,36} and hydride^{37,38} complexes of tungsten, molybdenum, tantalum, and zirconium. In most of these examples, the supported metal complex is in its highest oxidation state. To the best of our knowledge, however, the only supported low valent tungsten catalyst capable of effecting olefin metathesis is a supported organotungsten(IV) complex on silica, reported by Copéret and co-workers.^{39,40} Those authors propose that reduction of the silica supported W(VI) oxo generates a W(IV) species that can be readily reoxidized by an olefin to generate a catalytically relevant W(VI) alkylidene.

While the above studies paint a concise picture regarding the reactivity of unbound and supported organometallic complexes, there is a paucity of examples of systems bearing multimetallic motifs. Chisholm-type dimers of the form M_2X_6 (where $M = W$ and Mo ; $X =$ alkyl, alkoxide, and amide) have structural features that could have interesting implications for catalysis.⁴¹ The close proximity of the two metal centers, coupled with the electron reservoir of the metal–metal multiple bond, may allow for novel binding and reactivity which can be advantageous for catalysis.^{42,43} Studies targeting the chemical reactivity of free and supported metal dimers toward unsaturated hydrocarbons have been sporadic over the last few decades.^{44–49} For example, upon exposure to ethylene, the $W_2(O^iPr)_6$ dimer forms a bridging metalocyclic alkylidyne (Scheme 1).⁴⁵ However, isotopic labeling experiments indicate that no olefin metathesis occurs under these conditions.

Scheme 1. Pathway for the Reaction of $W_2(O^iPr)_6$ with Ethylene



$W_2(NMe_2)_6$ is unreactive toward unsaturated hydrocarbons; however, after deposition on silica it was shown to polymerize 1-heptyne, suggesting that chemisorption on silica can impart catalytic reactivity not observed for the molecular species.⁴⁶ Postsynthetic ligand substitution of the dimethylamide ligands with *tert*-butoxides was shown to produce an even more active catalyst.^{47,48} The discrepancy between the reactivity of the supported and unsupported tungsten dimers is likely due to either the electronic and/or steric effects exerted by the silanol ligand or the ability of the support to prevent the agglomeration of the active species which can lead to deactivation.

In an early example of supported organometallics, W_2Np_6 ($Np =$ neopentyl) was deposited onto silica and exhibited activity for olefin metathesis.⁵⁰ Unlike the unsupported parent, the silica supported, and thermally activated (at 100 °C) W_2Np_6 dimer was shown to catalyze the disproportionation of propene to ethylene and butenes. While these results were promising, structural characterization of the system was not reported, leaving the nature of the chemisorbed species undefined. Herein, we synthesized and supported a series of M_2X_6 ($M = W$ and Mo ; $X =$ alkyl, alkoxide, and amide) dimers on silica and used a combination of characterization techniques and density functional theory (DFT) calculations to elucidate the binding modes of the dimers on the surface and probe their activities toward olefin metathesis.

RESULTS AND DISCUSSION

Preparation of W_2Np_6 ($Np =$ neopentyl, **1) and Grafting onto SiO_{2-700} .** W_2Np_6 ($Np =$ neopentyl, **1**) was prepared according to a modified literature procedure (see the Supporting Information for details).⁴¹ A single crystal (Figure S1), grown from toluene at -30 °C, was found suitable for single crystal X-ray diffraction. The crystal structure of **1** revealed the classic D_{3d} arrangement with two tungsten atoms each coordinated by three neopentyl ligands and joined together via a multiple bond (Figure 1). The $W\equiv W$ bond length is

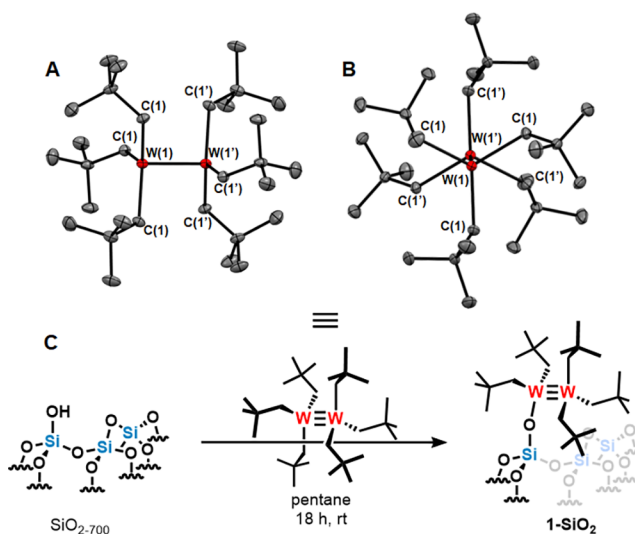


Figure 1. (A) Solid-state structure of **1** viewed perpendicular to the $W-W$ bond. (B) Solid-state structure of **1** viewed down to the $W-W$ bond highlighting the 3-fold axis. Thermal ellipsoids are drawn at 50% probability. Hydrogen atoms were omitted for clarity. Legend: tungsten (blue), carbon (gray). (C) Chemisorption of **1** onto SiO_{2-700} to yield **1-SiO₂**. Selected structural parameters: $W(1)-W(1') = 2.2440(5)$ Å, $W(1)-C(1) = 2.132(4)$ Å, $C(1)-W(1)-W(1') = 96.41(10)^\circ$, $C(1)-W(1)-C(1) = 118.77(4)^\circ$, $C(1)-W(1)-W(1')-C(1') = 60.0(10)^\circ$.

$2.244(1)$ Å, consistent with a triple bond. The $W\equiv W$ bond distance is the shortest reported for a homoleptic tungsten dimer and is similar to those of other $W\equiv W$ species.⁵² DFT confirmed the presence of a triple bond with a Mayer bond order of 3.6 (Table S10). UV–vis spectroscopy revealed a prominent absorption feature at 390 nm (Figure S2) associated with a $\pi \rightarrow \pi^*$ transition. This was supported by DFT (predicted transition at 404 nm). The Fourier transform infrared spectroscopy (FTIR) spectrum exhibited a set of vibrations around 2800 cm^{-1} assigned to the neopentyl $\nu(C-H)$ stretching frequencies. This assignment was supported by DFT calculations (Figure S3).

Addition of an orange solution of **1** in pentane to a suspension of partially dehydroxylated silica (Davisil-646, pretreated under vacuum at 700 °C, hydroxyl density⁵³ = 1.15 OH nm^{-2}) and mechanical agitation over the course of 15 h resulted in the deposition of **1** onto the silica support to produce an orange solid (**1-SiO₂**; 2.40 wt % W or 13.0 mmol/g via ICP) and a colorless supernatant solution. Tracking the deposition reaction by 1H NMR spectroscopy using 1,3,5-*tert*-Bu-benzene as an internal standard revealed the disappearance of starting material **1** (0.0077 mmol) and the appearance of approximately 1 equiv of neopentane (0.0055 mmol) with respect to **1**, suggesting that

1 chemisorbs to the silica via protonolysis, and that a Si–O–W bond is formed (Figure S4).

The ^1H solid-state nuclear magnetic resonance (SSNMR) spectrum of **1**-SiO₂ exhibited two peaks at 1.84 and 0.83 ppm, in a roughly 2:9 ratio, consistent with a neopentyl environment (Figure S5). Dynamic nuclear polarization (DNP)-enhanced SSNMR spectroscopy was used to elucidate the structure of the silica-supported tungsten dimer.^{54–56} The DNP-enhanced ^{13}C cross-polarization (CP) magic-angle-spinning (MAS) spectrum of the precatalyst is shown in Figure 2A. Resonances from the

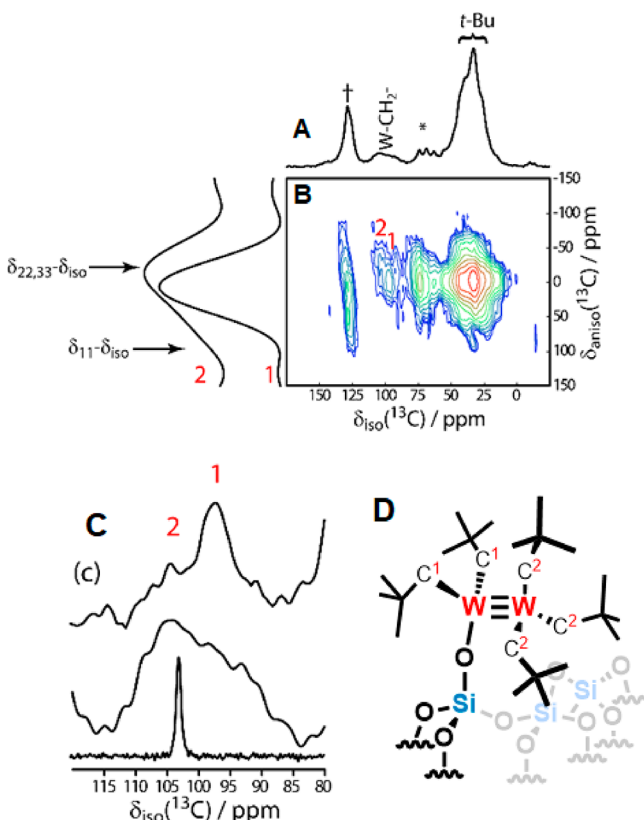


Figure 2. (A) DNP-enhanced ^{13}C CPMAS SSNMR spectrum of **1**-SiO₂. The dagger marks a benzene impurity and the asterisk marks residual protonated 1,1,2,2-tetrachloroethane (TCE); both are from the DNP solvent (TCE-*d*₂). (B) The 2D separation of undistorted powder patterns by effortless recoupling (SUPER) spectrum is shown along with projections along the two methylene resonances to highlight the difference in CSAs. The approximate principal components of the chemical shift tensor for site 2 are marked with arrows. (C) Enlarged views of the methylene region for the ^{13}C CPMAS spectra of crystalline **1** (bottom) and **1**-SiO₂ (middle), as well as the 1D projection of the 2D SUPER spectrum (top). (D) Assignment of the methylene carbon resonances distinguished in the 2D SUPER experiment.

large number of methyl groups are observed, as well as those of the metal bound methylene moieties, appearing as a broad resonance from 110 to 90 ppm. This resonance has an asymmetric line shape reminiscent of a pair of overlapping inequivalent resonances, as would be expected for the desymmetrized monopodal structure, as depicted in Figure 1C. The assignment was further supported by the similar ^{13}C NMR chemical shift observed for the methylene carbons in the molecular precursor in the solid-state (102.9 ppm, Figure 2C).⁴¹

A ^{13}C chemical shift anisotropy (CSA) recoupling measurement was performed to enhance the resolution and confirm that

two unique methylene environments are contributing to the signal at 100 ppm. The reasoning behind this choice of experiment was that small chemical shift changes due to changes in back-bonding do not influence all chemical shift tensor elements equally; rather, the one perpendicular to the metal–ligand bond, and the p orbital receiving the donation, is most strongly affected.^{41,57–61} This component is deshielded by increases in backbonding due to a stronger paramagnetic shielding contribution. A SUPER method was applied to measure the CSA.⁶² As can be seen in the 2D SUPER spectrum in Figure 2B, the two sites indeed have noticeably different CSAs, which confirms their assignments to electronically distinct metal centers (i.e., tungsten bound to silica or not), with the surface-bound site having the smaller CSA and the more distant site having an isotropic chemical shift that agreed with that of the molecular complex (Figure 2C). This difference in CSA skews the relative intensities in the 1D projection of the 2D SUPER spectrum (Figure 2C) from which the two types of neopentyl resonances can clearly be identified (Figure 2D). The higher chemical shift, stronger CSA, and negative skew of the C2 carbons all suggest that this site receives stronger back-donation from tungsten which is in agreement with its assignment to the neopentyl ligands coordinating to the tungsten that is not surface bound. This was independently confirmed through DFT calculations of the magnetic shielding tensors (Table S11).⁶³

X-ray absorption spectroscopy (XAS) was also used to verify that the W≡W bond in **1**-SiO₂ was still intact and to ascertain the coordination mode of the tungsten dimer on the silica (parameters can be found in Table 1). Upon grafting to silica,

Table 1. Selected EXAFS Parameters, along with Measured and Calculated Bond Lengths for **1** and **1**-SiO₂

	scattering path	R/Å	$\sigma^2/\times 10^{-3} \text{Å}^2$
1	W–C	2.163 (12)	2.3 (1.3)
	W≡W	2.259 (5)	1.8 (9)
1 -SiO ₂	W–C	2.117 (22)	21.5 (3.4)
	W≡W	2.285 (4)	2.7 (5)

the oxidation state of tungsten atoms in the surface species remained +3, as evident from the XANES data (Figure 3A). EXAFS fit results for **1** and **1**-SiO₂ were consistent with a model of a triple-bonded tungsten dimer (Figures 3B and S6–S9), with each tungsten bound to three ligands.

The W≡W dimer bond length is well-defined at 2.259(5) Å (Table 1), in good agreement with the single-crystal X-ray distance of 2.2440(5) Å. After tethering the molecule to the silica support, the two tungsten atoms are inequivalent, which complicated both the fitting and the interpretation. Although the data range beyond $k = 15 \text{Å}^{-1}$ allows for many independent points, or floating fit parameters, the correlations and uncertainties grow quite large for coordination number (*N*) and σ^2 . However, the W≡W dimer bond length was still measured at 2.285(4) Å, an elongation of 0.026 Å. DFT calculations were used to corroborate the structural assignments of **1** and **1**-SiO₂. W₂(Np)₅(OSiMe₃) serving as a surrogate to **1**-SiO₂ (Figure S10), the trimethylsilanol ligand (–OSiMe₃), was used as a computationally robust substitute for the silica surface. Attempts to independently synthesize a monosubstituted W₂(Np)₅(OR) model compound were unsuccessful due to the increased reactivity of the product to further protonolysis and disproportionation. The structures of **1** and **1**-SiO₂ were optimized using the M06-L⁶⁴ density functional and def2-

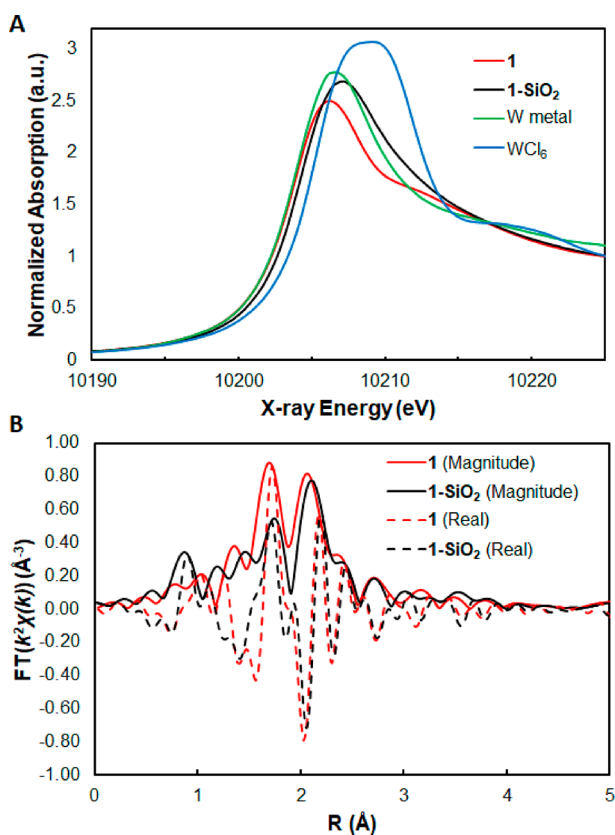


Figure 3. (A) XANES spectra of **1**, **1-SiO₂**, **WCl₆**, and tungsten foil. The relative positions of the edges and white lines support a conclusion of low-valent tungsten in the dimers. (B) Fourier transform magnitude (solid) and real (dashed) components of the EXAFS spectra for **1** (red) and **1-SiO₂** (black). The similarities in the real components indicate that the **W≡W** bond remains intact upon grafting to silica.

TZVPP^{65,66} basis set, implemented in Gaussian 09 package.⁶⁷ The geometry-optimized simulated structure of **1-SiO₂** exhibited an elongation of the **W≡W** bond compared to that of **1**, with an increase of 0.026 Å (from 2.298 to 2.324 Å) upon grafting onto silica (Table 2). The calculated elongation in the **W≡W** bond from **1** to **1-SiO₂** was consistent with the experimentally observed trend (Table 2).

UV resonance Raman spectroscopy was used to obtain information on the nature of the **W≡W** bond (Figure 4A). The Raman spectrum of **1** exhibited a sharp peak at 290 cm⁻¹ which was assigned to the **W≡W** stretching vibration. The spectrum of **1-SiO₂** exhibited a broader peak at 294 cm⁻¹ along with a

Table 2. **W≡W** Bond Lengths for **1** and **1-SiO₂** as Obtained from Various Techniques^a

complex (measurement)	W–W bond length/Å
1 (XRD)	2.244(1)
1 (XAS)	2.259(5)
1 (DFT)	2.298
1-SiO₂ (XAS)	2.285(4)
1-SiO₂ (DFT)	2.324
ΔW–W (XAS)	0.026(6)
ΔW–W (DFT)	0.026

^aThe agreement between the experimental results (XAS) and the simulated data (DFT) suggests that the **W≡W** bond lengths increase upon heterogenization onto a silica support.

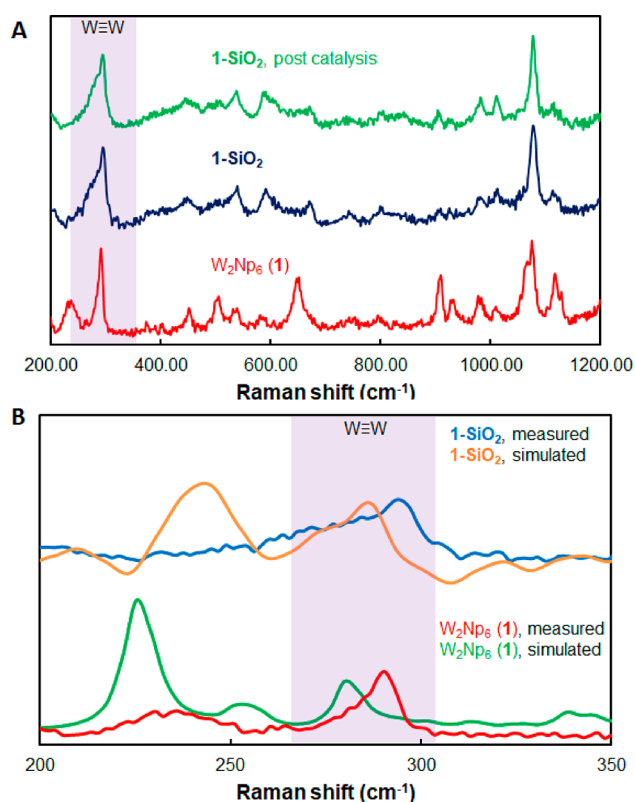


Figure 4. (A) UV resonance Raman spectra of **1**, **1-SiO₂**, and **1-SiO₂** postcatalysis (30 h on stream, *vide infra*) (red, blue, and green, respectively). The broadening of the **W≡W** vibration upon grafting to silica is consistent with the polarization of the triple bond, indicative of the monopodal binding of the dimer to the surface. (B) Overlays of the measured (red and blue) and simulated (green and orange) Raman spectra for **1** and **1-SiO₂**. The quantitative agreement between the experimental and simulated data strengthens the assignment of the **W≡W** triple bond. The simulated spectra were normalized with respect to the **W≡W** stretch.

shoulder at 278 cm⁻¹, evidencing interfacial interaction of the triple bond with silica, and appears to relate with the asymmetric broad resonance of the ¹³C NMR experiment (see Figure 2C). DFT calculations were employed to simulate the Raman spectra for **1** and **1-SiO₂**. The calculated **W≡W** stretches at 272 and 287 cm⁻¹ for **1-SiO₂** agreed with the observed values of 278 and 294 cm⁻¹, respectively (Figure 4B). These stretches were also consistent with previously reported ones.⁶⁸

1-SiO₂ was also characterized using diffuse reflectance infrared Fourier transform spectroscopy (DRIFTS). A DRIFTS spectrum of **1-SiO₂** showed the absorption bands in the range of 2870–2960 cm⁻¹ assigned to the $\nu(\text{C-H})$ stretching frequencies of the neopentyl ligands. This result was consistent with other literature examples.^{69–71} The simulated spectrum for **1-SiO₂** qualitatively matched the experimental spectrum (Figure S11). The measured UV–vis spectra of **1** and **1-SiO₂** and the simulated spectrum for **1-SiO₂** all showed a strong absorption at ~390 nm that was assigned to a $\pi \rightarrow \pi^*$ transition (Figure S2). High-angle annular dark field scanning transmission electron microscopy (HAADF-STEM) was used to ascertain the morphology of the surface species. **1-SiO₂** was heated to 100 °C under dynamic vacuum for 5 h to remove any adventitious organics that could interfere with the measurement. Raman and DRIFTS data suggested that the surface species remained intact post heat treatment (Figures S12 and S13). A STEM image of **1-**

SiO_2 (Figure 5A and S14) shows a collection of regions of high electron density (shown in yellow) corresponding to the

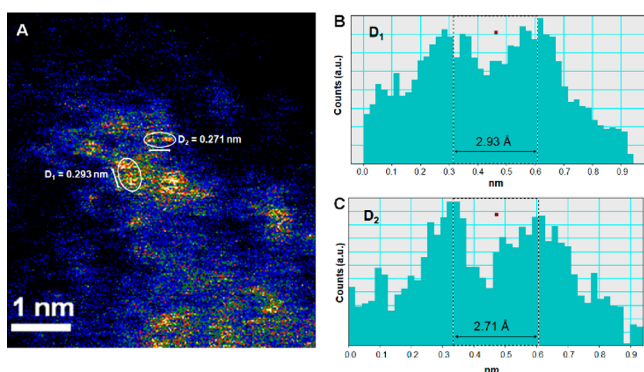
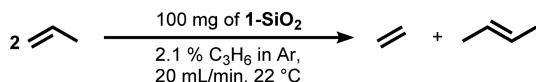


Figure 5. (A) STEM-HAADF image of 1-SiO_2 . The brightly colored yellow regions correspond to individual tungsten atoms. Circled in white are two pairs of tungsten dimers oriented perpendicular with respect to the electron beam. (B, C) Histograms of tungsten–tungsten separation extracted from the HAADF-STEM micrograph. The measured distances between the metal centers, D_1 and D_2 , were 2.71 and 2.91 Å, respectively.

tungsten atoms.^{72–75} Pairs of $\text{W}\equiv\text{W}$ oriented perpendicular to the electron beam are highlighted in white circles. The center-to-center distances between the tungsten atoms were measured at 2.71 and 2.91 Å (Figure 5B–C). These results suggest that the dimers are not agglomerated on the silica.

Catalytic Olefin Metathesis with 1-SiO_2 . The activity of 1-SiO_2 in the disproportionative self-metathesis of propylene was evaluated in an air-free plug flow reactor (Scheme 2). In a

Scheme 2. Reaction Scheme and Conditions for the Disproportionation of Propylene to Ethylene and 2-Butene



typical experiment, 100 mg of material was charged into a glass reactor tube (OD = 0.25 in., ID = 0.15 in.). Propylene (2.1% in argon) was fed into the reactor at a flow rate of 20 mL/min at room temperature ($\sim 22.0^\circ\text{C}$) over the course of 30 h. The gas outlet was connected to a gas chromatograph (GC-FID) which was used to identify and quantify the product profile of the mixture. These conditions were chosen in order to avoid operation at equilibrium conversion ($\sim 34\%$) and study the stability of the supported dimers.⁵¹

As seen in Figure 6, 1-SiO_2 is a competent propylene metathesis catalyst. At the start of the plug flow run, 1-SiO_2 exhibited a 5 h induction period as its conversion gradually increased from 6.6 to 19.8%. Similar profiles have been observed for other monometallic systems and are suggestive of the formation of a tungsten alkylidene moiety.⁶⁹ Following the induction period, 1-SiO_2 achieved a maximum performance of 20.0% conversion followed by a slow deactivation (16.0% conversion at 30 h). The product distribution of the reaction remained relatively constant with a *trans*-2-butene to *cis*-2-butene ratio of 2.3, consistent with the thermodynamic ratio.

Postcatalysis 1-SiO_2 (30 h on stream) was characterized using DRIFTS, Raman, and ^{13}C SSNMR spectroscopies. The persistence of the $\text{W}\equiv\text{W}$ in the Raman spectrum (Figure 4A), the $\nu(\text{C}-\text{H})$ stretches in the DRIFTS spectrum (Figure S15),

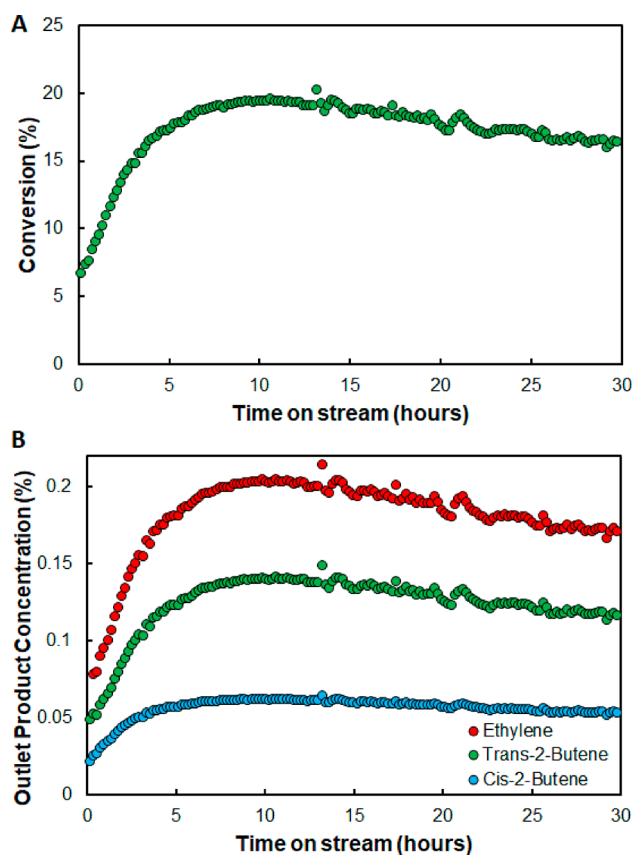
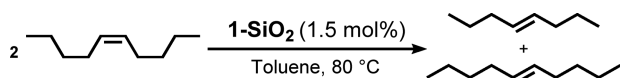


Figure 6. Reaction profiles for 1-SiO_2 during a 30 h plug flow run (top) and the product distribution of 1-SiO_2 throughout the 30 h period (bottom). Conditions: room temperature, 20 cc/min, 2% ethylene in argon. The parent complex, **1**, did not show any propensity toward metathesis.

and alkyl environments in the ^{13}C SSNMR spectrum (Figure S16) all suggest that the majority of the dimers on the surface remained intact after the 30 h plug flow experiment. Taken together, these observations suggest that the supported tungsten dimers are not quantitatively converted to an active alkylidene species. However, a pathway in which a trace amount of 1-SiO_2 is transformed into a highly active species cannot be ruled out. Thermogravimetric analysis (TGA) of 1-SiO_2 was employed in an attempt to observe the mass loss associated with α -elimination to produce neopentane (Figure S37). A mass loss at $\sim 100^\circ\text{C}$ could plausibly be assigned to the α -elimination. However, inspection of 1-SiO_2 thermolyzed at 100°C by DRIFTS and Raman spectroscopy did not identify any resonances that could be assigned to alkylidene species (Figures S12 and S13), and ^{13}C SSNMR of the post catalysis material, which had not deactivated significantly, also did not reveal an alkylidene resonance (Figure S16).

The activity of 1-SiO_2 toward solution-phase disproportionation of *cis*-4-nonene in toluene (0.26 M) at 80°C was also assessed (Scheme 3 and Figure 7). Sampling over the course of the first 25 min showed a low conversion rate indicative of an induction period consistent with observations in the flow reactor (3.5% conversion at 22 min). Following the induction period, the activity of the material ramped up, giving rise to a rapid increase in activity over the next 60 min after which point equilibrium was reached ($\sim 50\%$ conversion at the ca. 80 min mark). The reaction mixture was then filtered to remove 1-SiO_2 , and the metathesis activity of the supernatant solution was

Scheme 3. Reaction Scheme and Conditions for the Disproportionation of 4-Nonene to 4-Octene and 5-Decene^a



^aBoth cis and trans isomers are present in the reaction mixture.

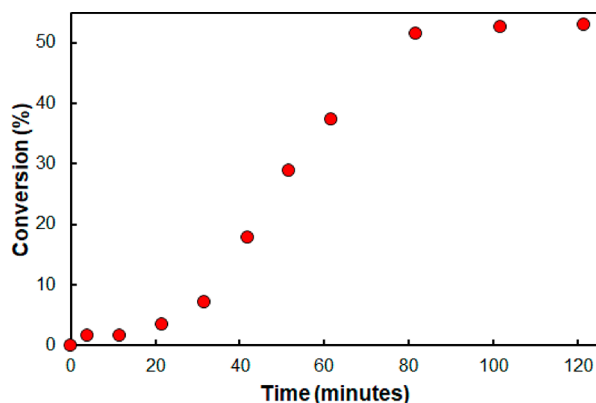


Figure 7. Plot of conversion over time for the disproportionation of nonene catalyzed by 1-SiO₂ in toluene at 80 °C to give octene and decene.

tested using fresh nonene. Sampling of the reaction mixture over the course of 10 h showed no change in the product distribution (Figure S17), confirming that the active species did not leach from 1-SiO₂ into the solution.⁷⁶ While the formation of catalytically active tungsten alkylidene species during the reaction cannot be ruled out, free neopentane, which would be diagnostic of such a process, was not detected in the reaction mixture.

Evaluation of Molybdenum Homologue. Mononuclear molybdenum complexes, both unsupported and supported, have also been extensively studied with regard to their olefin metathesis capabilities.^{35,77–79} In fact, well-defined molybdenum alkylidene complexes supported on silica are often more active for olefin metathesis than their tungsten homologues. The molybdenum analogue, Mo₂Np₆ (2), was prepared according to a modified literature procedure (see the Supporting Information for details) and grafted onto silica in a similar fashion to afford material 2-SiO₂ (Figure 8).

The UV–vis and FTIR spectra of 2 were qualitatively similar to those of 1 (Figures S18 and S19). ¹H NMR loading experiments under reaction conditions similar to those of 1-SiO₂ showed a decrease in the concentration of the Mo₂Np₆ dimer and the appearance of approximately 1 equiv of free neopentane, suggesting that 2 is also chemisorbed onto the silica via protonolysis and Si–O–Mo bond formation (Figure 8B and Figure S20) to yield a monopodal structure. ICP analysis of 2-SiO₂ confirmed a loading of 1.23% by mass or 12.8 mmol/g. The molar loading of molybdenum for 2-SiO₂ is comparable to the molar loading of tungsten in 1-SiO₂. A ¹H SSNMR spectrum of 2-SiO₂ revealed two peaks at 1.84 and 0.94 ppm, in a 2:9 ratio similar to the spectrum of 1-SiO₂ (Figure S21). Similarly, the DNP-enhanced ¹³C CPMAS NMR spectrum of 2-SiO₂ (Figure S22) featured resonances from both the *tert*-butyl carbons as well as the Mo-bound methylenes. In this case, the peak from the methylenes did not show the resolution of the two distinct environments, as was seen for 1-SiO₂, but the peak was broadened toward lower frequency, suggesting that the complex

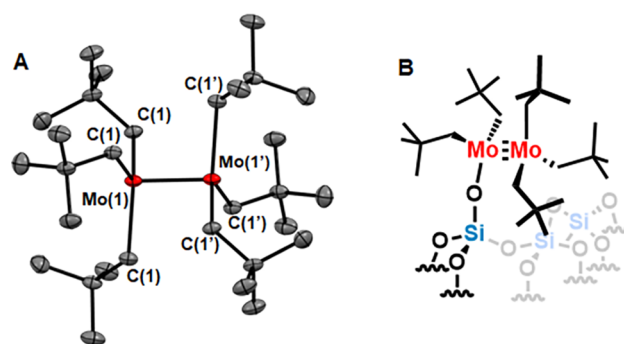


Figure 8. (A) Solid-state structure of 2 and (B) schematic of 2-SiO₂. Thermal ellipsoids are drawn at 50% probability. Hydrogen atoms were omitted for clarity. Legend: molybdenum (teal), carbon (gray). Selected structural parameters: Mo(1)–Mo(1') = 2.1654(7) Å, Mo(1)–C(1) = 2.148(2) Å, C(1)–Mo(1)–Mo(1') = 96.33(7)°, C(1)–Mo(1)–C(1) = 118.80(3)°, C(1)–Mo(1)–Mo(1')–C(1') = 60.0(10)°.

adopts a monopodal structure, like that seen for 1-SiO₂. 2-SiO₂ was also characterized by DRIFTS spectroscopy as exhibiting absorption bands in the range of 2870–2960 cm^{−1}, which were assigned to the ν (C–H) stretches of the neopentyl ligands (Figure S23). The DRIFTS of 1-SiO₂ and 2-SiO₂ were qualitatively similar suggesting that the materials are structurally analogous (Figure 11). A simulated DRIFTS spectrum for 2-SiO₂ matches the peak assignments (Figure S24). The UV–vis spectra of 2 and 2-SiO₂ were also qualitatively similar (Figure S18). Like the tungsten system, unsupported complex 2 is unreactive toward olefins, while 2-SiO₂ is active in the catalysis of metathesis reactions. Air-free propylene disproportionation plug flow experiments on 2-SiO₂ were carried out similarly to those of 1-SiO₂. Material 2-SiO₂ showed a different activity profile than that of 1-SiO₂ (Figure 9) with a maximum

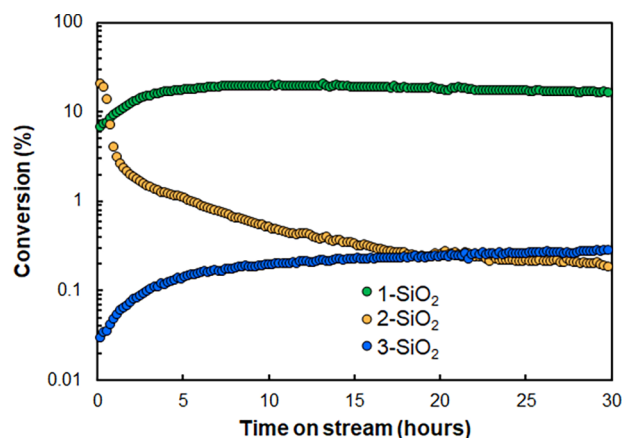


Figure 9. Reaction profiles for 1-SiO₂ (green), 2-SiO₂ (yellow), and 3-SiO₂ (blue). Conditions: room temperature, 20 cc/min, 2% ethylene in argon. Note that the y-axis is logarithmic.

conversion of 20.3% at the onset of the plug flow experiment. Soon thereafter, 2-SiO₂ experienced a drop in performance in the first 5 h (conversion rate of 1.0%) which did not recover for the rest of the run. The *trans*-/*cis*-butene ratio, while still favoring the thermodynamically more stable *trans* alkene, dropped from 3 to 1.4, as the plug flow run commenced (Figure S24).

Effect of the Ancillary Ligand. The metathesis activities of **1-SiO₂** and **2-SiO₂** were hypothesized to proceed through a pathway that involves a neopentylidene generated by α -elimination. To test this hypothesis, *tert*-butoxide ($W_2(O^tBu)_6$ and $Mo_2(O^tBu)_6$, **3** and **4**, respectively) and dimethylamide ($W_2(NMe_2)_6$ and $Mo_2(NMe_2)_6$, **5** and **6**, respectively) ligated dimers, were grafted onto silica and investigated by procedures analogous to **1** and **2** (Figure 10).

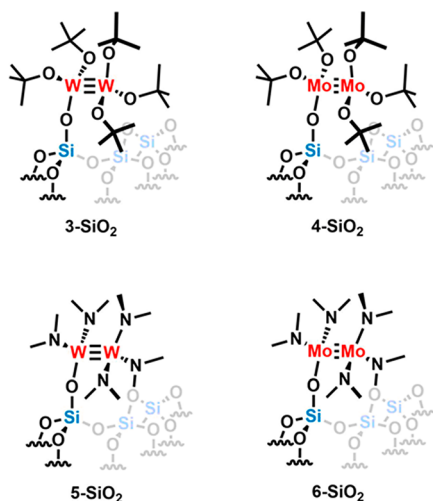


Figure 10. Structures of (3–6)-SiO₂.

The grafting of **3–6** proceeded in accordance to the techniques employed for **1** and **2**. ¹H NMR loading experiments under similar reaction conditions to those of **1-SiO₂** showed the disappearance of **3–6** over the course of 1 h, but neither *tert*-butanol nor dimethylamine was observed (Figures S25, S27, S29, and S31). This can be explained by the physisorption of the protonated ligand onto the silica, as previously observed.⁷² The results of the ICP analysis of the grafted materials (3–6)-SiO₂ can be found in Table 3. The metal loading was roughly 13 mmol/g for all the systems.

Table 3. ICP Data for Materials (1–6)-SiO₂

material	metal	wt %	mmol/g
1-SiO ₂	W	2.40	13.0
2-SiO ₂	Mo	1.23	12.8
3-SiO ₂	W	2.78	15.1
4-SiO ₂	Mo	1.30	13.6
5-SiO ₂	W	2.33	12.6
6-SiO ₂	Mo	1.29	13.5

The ¹H SSNMR spectra of **3-SiO₂** and **4-SiO₂** exhibited a broad singlet in the 1.00–2.00 ppm range consistent with an asymmetric binding mode to the surface (Figures S26 and S28). The DRIFTS spectra for **3-SiO₂** and **4-SiO₂** had motifs similar to those of **1-SiO₂** and **2-SiO₂** to which they are structurally analogous (Figure 11). **5-SiO₂** was previously prepared and characterized and thus was used as a reference.⁴⁶ The ¹H SSNMR spectrum of **5-SiO₂** exhibited a broad multiplet in the 0–5 ppm range (Figure S30). This was consistent with a rotationally locked dimer on the surface and agreed with the previously reported spectrum for **5-SiO₂**.⁴⁷ DRIFTS characterization of **5-SiO₂** revealed a series of peaks in the range of 2760–3000 cm⁻¹ attributed to the $\nu(C-H)$ stretches of the

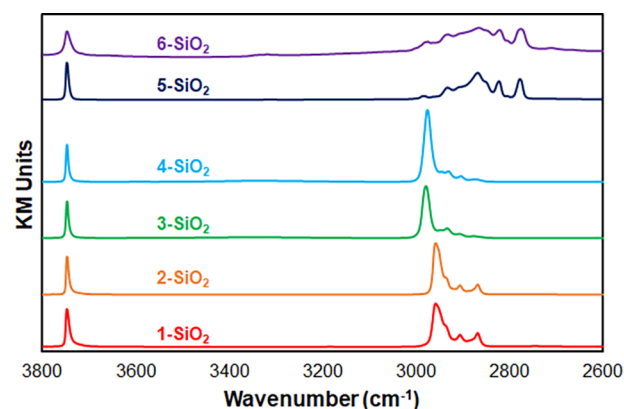


Figure 11. DRIFTS spectra for (1–6)-SiO₂ normalized to the intensity of the silica peak at 3750 cm⁻¹.

dimethylamine ligand (Figure 11).⁴⁷ Finally, the ¹H SSNMR and DRIFTS spectra of **6-SiO₂** were qualitatively similar to those of **5-SiO₂**, suggesting that **6-SiO₂** was the Mo homologue of **5-SiO₂** (Figures 11 and S32). These data suggest that **3–6** were successfully chemisorbed onto the silica surface and were coordinated to the metal centers in a monopodal fashion.

Air-free propylene disproportionation plug flow experiments with materials (3–6)-SiO₂ were run in a fashion similar to those on (1, 2)-SiO₂. Out of the four materials, only **3-SiO₂** catalyzed the metathesis of propene (Figures 10 and S33), albeit with much lower activity compared to the alkyl congeners. With an initial conversion of 0.03%, the activity of **3-SiO₂** gradually increased over the course of 30 hours at which point it reached a conversion of 0.28% (Figure S33). The trans/cis ratio for the formed products was close to unity for the duration of the experiment, likely reflecting the kinetic product selectivity at low conversion (Figures S33 and S34). Upon removal of **3-SiO₂** from the plug flow reactor, a distinct color change from red to black was observed, suggestive of the formation of a new species upon exposure to the reactant stream; no other materials in this report demonstrated such a change. The activity, or lack thereof, observed for (3–6)-SiO₂ supports the hypothesis that the metathesis reaction proceeds through a metal–neopentylidene intermediate, formed via H- α -elimination from a neopentyl group.

CONCLUSION

In this work, we investigated the reactivity of a family of silica supported tungsten and molybdenum dimers toward olefin metathesis. Using a combination of spectroscopic techniques, it was shown that for all six compounds, chemisorption occurs by a protonolysis reaction to release 1 equiv of ligand per metal complex, resulting in a monopodal surface organometallic species. In contrast with its molecular parent, **1-SiO₂** is a competent metathesis catalyst in both plug flow (propylene) and batch (nonene) reactor modes, making it the first example of a well-defined system featuring a supported W(III) precatalyst. The reactivity observed for alkyl complexes (1–2)-SiO₂ compared to those observed for alkoxide and amide complexes (3–6)-SiO₂, coupled with the induction period for **1-SiO₂**, are consistent with a mechanism which proceeds through the formation of a neopentylidene generated by α -elimination, although other mechanisms of alkylidene formation are plausible. The discrepancy between the reactivity of **1** and **1-SiO₂** could be explained by the lowering of the activation barrier

of **1** through the electronic effects of the silanol ligand or by site isolation of reactive intermediates on the surface.⁸⁰ More detailed experimental and computational investigations into the mechanism by which 1-SiO₂ catalyzes the metathesis of propylene are underway.

■ ASSOCIATED CONTENT

Supporting Information

The Supporting Information is available free of charge at <https://pubs.acs.org/doi/10.1021/acs.organomet.9b00787>.

General discussion of synthetic and experimental procedures, instrumentation, characterization of materials, and rate laws and their derivations (PDF)

XYZ coordinate files for computational assessment of ligand displacement from vanadium to support mechanistic discussion (ZIP)

Accession Codes

CCDC 1968533–1968534 contain the supplementary crystallographic data for this paper. These data can be obtained free of charge via www.ccdc.cam.ac.uk/data_request/cif, or by emailing data_request@ccdc.cam.ac.uk, or by contacting The Cambridge Crystallographic Data Centre, 12 Union Road, Cambridge CB2 1EZ, UK; fax: +44 1223 336033.

■ AUTHOR INFORMATION

Corresponding Authors

Alfred P. Sattelberger – Chemical Sciences and Engineering Division, Argonne National Laboratory, Lemont, Illinois 60439, United States; Email: asattelberger@anl.gov

David M. Kaphan – Chemical Sciences and Engineering Division, Argonne National Laboratory, Lemont, Illinois 60439, United States; orcid.org/0000-0001-5293-7784; Email: kaphand@anl.gov

Massimiliano Delferro – Chemical Sciences and Engineering Division, Argonne National Laboratory, Lemont, Illinois 60439, United States; orcid.org/0000-0002-4443-165X; Email: delferro@anl.gov

Authors

Alon Chapovetsky – Chemical Sciences and Engineering Division, Argonne National Laboratory, Lemont, Illinois 60439, United States

Ryan R. Langeslay – Chemical Sciences and Engineering Division, Argonne National Laboratory, Lemont, Illinois 60439, United States; orcid.org/0000-0003-2915-9309

Gokhan Celik – Chemical Sciences and Engineering Division, Argonne National Laboratory, Lemont, Illinois 60439, United States; orcid.org/0000-0001-8070-5219

Frédéric A. Perras – U.S. DOE Ames Laboratory, Ames, Iowa 50011, United States; orcid.org/0000-0002-2662-5119

Marek Pruski – U.S. DOE Ames Laboratory, Ames, Iowa 50011, United States; Department of Chemistry, Iowa State University, Ames, Iowa 50011, United States; orcid.org/0000-0001-7800-5336

Magali S. Ferrandon – Chemical Sciences and Engineering Division, Argonne National Laboratory, Lemont, Illinois 60439, United States

Evan C. Wegener – Chemical Sciences and Engineering Division, Argonne National Laboratory, Lemont, Illinois 60439, United States

Hacksung Kim – Chemical Sciences and Engineering Division, Argonne National Laboratory, Lemont, Illinois 60439, United States

States; Center for Catalysis and Surface Science and Department of Chemistry, Northwestern University, Evanston, Illinois 60208, United States; orcid.org/0000-0002-5599-065X

Fulya Dogan – Chemical Sciences and Engineering Division, Argonne National Laboratory, Lemont, Illinois 60439, United States; orcid.org/0000-0001-7997-266X

Jianguo Wen – Center for Nanoscale Materials, Argonne National Laboratory, Lemont, Illinois 60439, United States; orcid.org/0000-0002-3755-0044

Navneet Khetrpal – Department of Chemistry, Chemical Theory Center, and Supercomputing Institute, University of Minnesota, Minneapolis, Minnesota 55455, United States

Prachi Sharma – Department of Chemistry, Chemical Theory Center, and Supercomputing Institute, University of Minnesota, Minneapolis, Minnesota 55455, United States; orcid.org/0000-0002-1819-542X

Jacob White – Department of Chemistry, Chemical Theory Center, and Supercomputing Institute, University of Minnesota, Minneapolis, Minnesota 55455, United States

A. Jeremy Kropf – Chemical Sciences and Engineering Division, Argonne National Laboratory, Lemont, Illinois 60439, United States

Complete contact information is available at:

<https://pubs.acs.org/doi/10.1021/acs.organomet.9b00787>

Funding

This work was supported by the U.S. Department of Energy (DOE), Office of Basic Energy Sciences, Division of Chemical Sciences, Geosciences, and Biosciences, Catalysis Science Program under contract nos. DE-AC-02-06CH11357 (Argonne National Laboratory) and DE-AC02-07CH11358 (Ames Laboratory). Use of the Advanced Photon Source was supported by the U.S. DOE, Office of Science, and Office of the Basic Energy Sciences, under contract no. DE-AC-02-06CH11357. MRCAT operations were supported by the DOE and the MRCAT member institutions. Use of the TEM at the Center for Nanoscale Materials at Argonne National Laboratory is supported by the U.S. Department of Energy, Office of Science, Office of Basic Energy Sciences, under contract no. DE-AC-02-06CH11357. The computational work was supported by the Inorganometallic Catalyst Design Center, an EFRC funded by the DOE, Office of Basic Energy Sciences (DE-SC0012702). P.S. acknowledges a doctoral dissertation fellowship from the University of Minnesota. H.K. (UV Raman work) was supported by the US Department of Energy, Office of Basic Energy Sciences, through grant no. DE-FG02-03ER15457 to the Institute for Catalysis for Energy Processes (ICEP) at Northwestern University. F.K.D. acknowledges support from the Vehicle Technologies Office at the U.S. Department of Energy Efficiency and Renewable Energy

Notes

The authors declare no competing financial interest.

■ ACKNOWLEDGMENTS

We thank Laura Gagliardi (University of Minnesota) for useful discussions and Charlotte Stern (Northwestern University) for crystallographic support. We also thank Tom Gilbert (Northern Illinois University) for helpful discussions on the M₂Np₆ syntheses.

REFERENCES

- (1) Grubbs, R. H.; Wenzel, A. G.; O'Leary, D. J.; Khosravi, E. *Handbook of Metathesis*; Wiley-VCH, 2015; p 1.
- (2) Nguyen, T. T.; Koh, M. J.; Shen, X.; Romiti, F.; Schrock, R. R.; Hoveyda, A. H. Kinetically controlled E-selective catalytic olefin metathesis. *Science* **2016**, *352*, 569.
- (3) Ertl, G.; Knözinger, H.; Schuth, F.; Weitkamp, J., Eds. *Handbook of Heterogeneous Catalysis*; Wiley-VCH, 2008.
- (4) Sheldon, R. A.; van Bekkum, H., Eds. *Fine Chemicals through Heterogeneous Catalysis*; Wiley-VCH, 2007.
- (5) Mol, J. C. Industrial applications of olefin metathesis. *J. Mol. Catal. A: Chem.* **2004**, *213* (1), 39–45.
- (6) Copéret, C.; Comas-Vives, A.; Conley, M. P.; Estes, D.; Nunez-Zarur, F.; Fedorov, A.; Mougél, V.; Nagae, H.; Zhizhko, P. A. Surface Organometallic and Coordination Chemistry towards Single-Site Heterogeneous Catalysts: Strategies, Methods, Structures, and Activities. *Chem. Rev.* **2016**, *116*, 323–421.
- (7) Stalzer, M. M.; Delferro, M.; Marks, T. J. Supported Single-Site Organometallic Catalysts for the Synthesis of High-Performance Polyolefins. *Catal. Lett.* **2015**, *145*, 3–14.
- (8) Williams, L. A.; Guo, N.; Motta, A.; Delferro, M.; Fragala, I. L.; Miller, J. T.; Marks, T. J. Surface Structural-Chemical Characterization of a Single-Site d^0 Heterogeneous Arene Hydrogenation Catalyst Having 100% Active Sites. *Proc. Natl. Acad. Sci. U. S. A.* **2013**, *110*, 413–418.
- (9) Rendon, N.; Berthoud, R.; Blanc, F.; Gajan, D.; Maishal, T.; Basset, J. M.; Coperet, C.; Lesage, A.; Emsley, L.; Marinescu, S. C.; et al. Well-Defined Silica-Supported Mo-Alkylidene Catalyst Precursors Containing One OR Substituent: Methods of Preparation and Structure-Reactivity Relationship in Alkene Metathesis. *Chem. - Eur. J.* **2009**, *15*, 5083–5089.
- (10) Candy, J. P.; Copéret, C.; Basset, J. M. Analogy between Surface and Molecular Organometallic Chemistry. *Top. Organomet. Chem.* **2005**, *16*, 151–210.
- (11) Wegener, S. L.; Marks, T. J.; Stair, P. C. Design Strategies for the Molecular Level Synthesis of Supported Catalysts. *Acc. Chem. Res.* **2012**, *45*, 206–214.
- (12) Williams, L. A.; Marks, T. J. Synthesis, Characterization, and Heterogeneous Catalytic Implementation of Sulfated Alumina Nanoparticles. Arene Hydrogenation and Olefin Polymerization Properties of Supported Organozirconium Complexes. *ACS Catal.* **2011**, *1*, 238–245.
- (13) Nicholas, C. P.; Marks, T. J. Sulfated Tin Oxide Nanoparticles as Supports for Molecule-Based Olefin Polymerization Catalysts. *Nano Lett.* **2004**, *4*, 1557–1558.
- (14) Nicholas, C. P.; Marks, T. J. Zirconium Hydrocarbyl Chemisorption on Sulfated Metal Oxides: New Supports, Chemisorption Pathways, and Implications for Catalysis. *Langmuir* **2004**, *20*, 9456–9462.
- (15) Nicholas, C. P.; Ahn, H.; Marks, T. J. Synthesis, Spectroscopy, and Catalytic Properties of Cationic Organozirconium Adsorbates on "Super Acidic" Sulfated Alumina. "Single-Site" Heterogeneous Catalysts with Virtually 100% Active Sites. *J. Am. Chem. Soc.* **2003**, *125*, 4325–4331.
- (16) Hu, B.; Getsoian, A.; Schweitzer, N. M.; Das, U.; Kim, H.; Niklas, J.; Poluektov, O.; Curtiss, L. A.; Stair, P. C.; Miller, J. T.; et al. Selective Propane Dehydrogenation with Single-Site Co^{II} on SiO_2 by a Non-Redox Mechanism. *J. Catal.* **2015**, *322*, 24–37.
- (17) Mazoyer, E.; Szeto, K. C.; Merle, N.; Thivolle-Cazat, J.; Boyron, O.; Basset, J. M.; Nicholas, C. P.; Taoufik, M. Insights into the Deactivation Mechanism of Supported Tungsten Hydride on Alumina ($\text{W-H}/\text{Al}_2\text{O}_3$) Catalyst for the Direct Conversion of Ethylene to Propylene. *J. Mol. Catal. A: Chem.* **2014**, *385*, 125–132.
- (18) Pasha, F. A.; Cavallo, L.; Basset, J. M. Mechanism of n-Butane Hydrogenolysis Promoted by Ta-Hydrides Supported on Silica. *ACS Catal.* **2014**, *4*, 1868–1874.
- (19) Solans-Monfort, X.; Chow, C.; Gouré, E.; Kaya, Y.; Basset, J. M.; Taoufik, M.; Quadrelli, E. A.; Eisenstein, O. Successive Heterolytic Cleavages of H_2 Achieve N_2 Splitting on Silica-Supported Tantalum Hydrides: A DFT Proposed Mechanism. *Inorg. Chem.* **2012**, *51*, 7237–7249.
- (20) Pelletier, J.; Espinas, J.; Vu, N.; Norsic, S.; Baudouin, A.; Delevoye, L.; Trebosc, J.; Le Roux, E.; Santini, C.; Basset, J. M.; et al. A Well-Defined Silica-Supported Aluminium Alkyl through an Unprecedented, Consecutive Two-Step Protonolysis-Alkyl Transfer Mechanism. *Chem. Commun.* **2011**, *47*, 2979–2981.
- (21) Arteaga-Müller, R.; Tsurugi, H.; Saito, T.; Yanagawa, M.; Oda, S.; Mashima, K. New Tantalum Ligand-Free Catalyst System for Highly Selective Trimerization of Ethylene Affording 1-Hexene: New Evidence of a Metallacycle Mechanism. *J. Am. Chem. Soc.* **2009**, *131*, 5370–5371.
- (22) Brutchey, R. L.; Ruddy, D. A.; Andersen, L. K.; Tilley, T. D. Influence of Surface Modification of Ti-SBA15 Catalysts on the Epoxidation Mechanism for Cyclohexene with Aqueous Hydrogen Peroxide. *Langmuir* **2005**, *21*, 9576–9583.
- (23) Agapie, T.; Schofer, S. J.; Labinger, J. A.; Bercaw, J. E. Mechanistic Studies of the Ethylene Trimerization Reaction with Chromium-Diphosphine Catalysts: Experimental Evidence for a Mechanism Involving Metallacyclic Intermediates. *J. Am. Chem. Soc.* **2004**, *126*, 1304–1305.
- (24) Farcasiu, D.; Ghenciu, A.; Li, J. Q. The Mechanism of Conversion of Saturated Hydrocarbons Catalyzed by Sulfated Metal Oxides: Reaction of Adamantane on Sulfated Zirconia. *J. Catal.* **1996**, *158*, 116–117.
- (25) Mougél, V.; Santiago, C. B.; Zhizhko, P. A.; Bess, E. N.; Varga, J.; Frater, G.; Sigman, M. S.; Coperet, C. Quantitatively Analyzing Metathesis Catalyst Activity and Structural Features in Silica-Supported Tungsten Imido-Alkylidene Complexes. *J. Am. Chem. Soc.* **2015**, *137*, 6699–6704.
- (26) Allouche, F.; Mougél, V.; Copéret, C. Activating Thiolate-Based Imidoalkylidene Tungsten(VI) Metathesis Catalysts by Grafting onto Silica. *Asian J. Org. Chem.* **2015**, *4*, 528–532.
- (27) Conley, M. P.; Mougél, V.; Peryshkov, D. V.; Forrest, W. P.; Gajan, D.; Lesage, A.; Emsley, L.; Coperet, C.; Schrock, R. R. A Well-Defined Silica-Supported Tungsten Oxo Alkylidene Is a Highly Active Alkene Metathesis Catalyst. *J. Am. Chem. Soc.* **2013**, *135*, 19068–19070.
- (28) Beaudoin, M. C.; Womiloju, O.; Fu, A. Q.; Ajjou, J. A. N.; Rice, G. L.; Scott, S. L. Silica-Supported Alkylidene Complexes: Their Preparation, Characterization and Reactivity, Especially towards Olefins. *J. Mol. Catal. A: Chem.* **2002**, *190*, 159–169.
- (29) Copéret, C.; Maury, O.; Thivolle-Cazat, J.; Basset, J. M. σ -Bond Metathesis of Alkanes on a Silica-Supported Tantalum(V) Alkyl Alkylidene Complex: First Evidence for Alkane Cross-Metathesis. *Angew. Chem., Int. Ed.* **2001**, *40*, 2331–2334.
- (30) Crozier, A. R.; Schadle, C.; Maichle-Mossmeyer, C.; Tornroos, K. W.; Anwander, R. Synthesis and Grafting of CAN-Derived Tetravalent Cerium Alkoxide Silylamide Precursors onto Mesoporous Silica MCM-41. *Dalton Trans.* **2013**, *42*, 5491–5499.
- (31) Bouhoute, Y.; Garron, A.; Grekov, D.; Merle, N.; Szeto, K. C.; De Mallmann, A.; Del Rosal, I.; Maron, L.; Girard, G.; Gauvin, R. M.; et al. Well-Defined Supported Mononuclear Tungsten Oxo Species as Olefin Metathesis Pre-Catalysts. *ACS Catal.* **2014**, *4*, 4232–4241.
- (32) Chen, Y.; Abou-Hamad, E.; Hamieh, A.; Hamzaoui, B.; Emsley, L.; Basset, J. M. Alkane Metathesis with the Tantalum Methylidene $[(\equiv\text{SiO})\text{Ta}(\text{=CH}_2)\text{Me}_2]/[(\equiv\text{SiO})_2\text{Ta}(\text{=CH}_2)\text{Me}]$ Generated from Well-Defined Surface Organometallic Complex $[(\equiv\text{SiO})\text{Ta}^{\text{V}}\text{Me}_4]$. *J. Am. Chem. Soc.* **2015**, *137*, 588–591.
- (33) Mougél, V.; Santiago, C. B.; Zhizhko, P. A.; Bess, E. N.; Varga, J.; Frater, G.; Sigman, M. S.; Copéret, C. Quantitatively Analyzing Metathesis Catalyst Activity and Structural Features in Silica-Supported Tungsten Imido-Alkylidene Complexes. *J. Am. Chem. Soc.* **2015**, *137*, 6699–6704.
- (34) Zhizhko, P. A.; Zhizhin, A. A.; Belyakova, O. A.; Zubavichus, Y. V.; Kolyagin, Y. G.; Zarubin, D. N.; Ustynuk, N. A. Oxo/Imido Heterometathesis Reactions Catalyzed by a Silica-Supported Tantalum Imido Complex. *Organometallics* **2013**, *32*, 3611–3617.

- (35) Townsend, E. M.; Hyvl, J.; Forrest, W. P.; Schrock, R. R.; Müller, P.; Hoveyda, A. H. Synthesis of Molybdenum and Tungsten Alkylidene Complexes That Contain Sterically Demanding Arenethiolate Ligands. *Organometallics* **2014**, *33*, 5334–5341.
- (36) Conley, M. P.; Mougel, V.; Peryshkov, D. V.; Forrest, W. P.; Gajan, D.; Lesage, A.; Emsley, L.; Copéret, C.; Schrock, R. R. A Well-Defined Silica-Supported Tungsten Oxo Alkylidene Is a Highly Active Alkene Metathesis Catalyst. *J. Am. Chem. Soc.* **2013**, *135*, 19068–19070.
- (37) Soignier, S.; Taoufik, M.; Le Roux, E.; Saggio, G.; Dablemont, C.; Baudouin, A.; Lefebvre, F.; de Mallmann, A.; Thivolle-Cazat, J.; Basset, J. M.; et al. Tantalum Hydrides Supported on MCM-41 Mesoporous Silica: Activation of Methane and Thermal Evolution of the Tantalum-Methyl Species. *Organometallics* **2006**, *25*, 1569–1577.
- (38) Pasha, F. A.; Bendjeriou-Sedjerari, A.; Huang, K. W.; Basset, J. M. C-H and C-C Activation of n-Butane with Zirconium Hydrides Supported on SBA15 Containing N-Donor Ligands: [(≡SiNH)(≡SiX)ZrH₂], [(≡SiNH)(≡SiX)₂ZrH], and [(≡SiN=)(≡SiX)₂ZrH] (X = -NH₂, -O-). A DFT Study. *Organometallics* **2014**, *33*, 3320–3327.
- (39) Mougel, V.; Chan, K.-W.; Siddiqi, G.; Kawakita, K.; Nagae, H.; Tsurugi, H.; Mashima, K.; Safonova, O.; Copéret, C. Low Temperature Activation of Supported Metathesis Catalysts by Organosilicon Reducing Agents. *ACS Cent. Sci.* **2016**, *2* (8), 569–576.
- (40) Chan, K. W.; Mance, D.; Safonova, O. V.; Copéret, C. Well-Defined Silica-Supported Tungsten(IV)-Oxo Complex: Olefin Metathesis Activity, Initiation, and Role of Brønsted Acid Sites. *J. Am. Chem. Soc.* **2019**, *141* (45), 18286–18292.
- (41) Chisholm, M. H.; Eichhorn, B. W.; Foltling, K.; Huffman, J. C.; Ontiveros, C. D.; Streib, W. E.; Van der Sluys, W. G. Preparation and characterization of sodium heptachloropentakis(THF)ditungstate⁽¹⁻⁾. A synthetically useful precursor for X₂W≡WX₃ compounds where X = CH₂-tert-Bu, NMe₂ and O-tert-Bu. *Inorg. Chem.* **1987**, *26* (19), 3182–3186.
- (42) Schrock, R. R.; Lopez, L. P. H.; Hafer, J.; Singh, R.; Sinha, A.; Müller, P. Olefin Metathesis Reactions Initiated by d² Molybdenum or Tungsten Complexes. *Organometallics* **2005**, *24* (22), 5211–5213.
- (43) Tooze, R. P.; Motevalli, M.; Hursthouse, M. B.; Wilkinson, G. Alkyl compounds of diruthenium(III) and osmium(III). X-Ray crystal structure of the first ruthenium peralkyl, hexakis(neopentyl)diruthenium(III). *J. Chem. Soc., Chem. Commun.* **1984**, No. 12, 799–800.
- (44) Taha, Z. A.; Deguns, E. W.; Chattopadhyay, S.; Scott, S. L. Formation of Digallium Sites in the Reaction of Trimethylgallium with Silica. *Organometallics* **2006**, *25* (8), 1891–1899.
- (45) Chisholm, M. H.; Huffman, J. C.; Hampden-Smith, M. J. Metal alkoxides. Models for metal oxides. 15. Carbon-carbon and carbon hydrogen bond activation in the reactions between ethylene and ditungsten hexaalkoxides: W₂(OCH₂-t-Bu)₆(.eta.-₂-C₂H₄)₂, W₂(OR)₆(CH₂)₄(.eta.-₂-C₂H₄), and W₂(OR)₆(.mu.-CCH₂CH₂CH₂) (where R = CH₂-t-Bu, i-Pr, c-C₅H₉, and c-C₆H₁₁). Preparations, properties, structures, and reaction mechanisms. *J. Am. Chem. Soc.* **1989**, *111* (14), 5284–5299.
- (46) Coutelier, O.; Nowogrocki, G.; Paul, J.-F.; Mortreux, A. Selective Terminal Alkyne Metathesis: Synthesis and Use of a Unique Triple Bonded Dinuclear Tungsten Alkoxy Complex Containing a Hemilabile Ligand. *Adv. Synth. Catal.* **2007**, *349* (14–15), 2259–2263.
- (47) Gauvin, R. M.; Coutelier, O.; Berrier, E.; Mortreux, A.; Delevoe, L.; Paul, J. F.; Mamede, A. S.; Payen, E. A Well-Defined Silica-Supported Dinuclear Tungsten(III) Amido Species: Synthesis, Characterization and Reactivity. *Dalton Trans.* **2007**, 3127–3130.
- (48) Coutelier, O.; Gauvin, R. M.; Nowogrocki, G.; Trebosc, J.; Delevoe, L.; Mortreux, A. A New Donor-Stabilized Ditungsten Amido Alkoxido Species: Synthesis, Crystal Structure, Fluxionality, and Grafting onto Silica. *Eur. J. Inorg. Chem.* **2007**, 5541–5547.
- (49) Zhao, Y.; Yang, K. R.; Wang, Z.; Yan, X.; Cao, S.; Ye, Y.; Dong, Q.; Zhang, X.; Thorne, J. E.; Jin, L.; Materna, K. L.; Trimpalis, A.; Bai, H.; Fakra, S. C.; Zhong, X.; Wang, P.; Pan, X.; Guo, J.; Flytzani-Stephanopoulos, M.; Brudvig, G. W.; Batista, V. S.; Wang, D. Stable iridium dinuclear heterogeneous catalysts supported on metal-oxide substrate for solar water oxidation. *Proc. Natl. Acad. Sci. U. S. A.* **2018**, *115* (12), 2902–2907.
- (50) Smith, J.; Mowat, W.; Whan, D. A.; Ebsworth, E. A. V. Organometallic Complexes of Molybdenum and Tungsten as Catalyst Precursors in the Disproportionation of Propene. *J. Chem. Soc., Dalton Trans.* **1974**, 1742–1746.
- (51) Van de Graaf, J. M.; Zwiép, M.; Kapteijn, F.; Moulijn, J. A. Application of a zeolite membrane reactor in the metathesis of propene. *Chem. Eng. Sci.* **1999**, *54* (10), 1441–1445.
- (52) Cotton, F. A.; Murillo, A. M.; Walton, R. A., Eds. *Multiple Bonds between Metal Atoms*, 3rd ed.; Springer Science and Business Media Inc.: New York, 2005.
- (53) Zhuravlev, L. T. The Surface Chemistry of Amorphous Silica. Zhuravlev Model. *Colloids Surf., A* **2000**, *173*, 1–38.
- (54) Lesage, A.; Lelli, M.; Gajan, D.; Caporini, M. A.; Vitzthum, V.; Miéville, P.; Alauzun, J.; Roussey, A.; Thieuleux, C.; Mehdi, A.; et al. Surface Enhanced NMR Spectroscopy by Dynamic Nuclear Polarization. *J. Am. Chem. Soc.* **2010**, *132*, 15459–15461.
- (55) Rossini, A. J.; Zagdoun, A.; Lelli, M.; Lesage, A.; Copéret, C.; Emsley, L. Dynamic Nuclear Polarization Surface Enhanced NMR Spectroscopy. *Acc. Chem. Res.* **2013**, *46*, 1942–1951.
- (56) Kobayashi, T.; Perras, F. A.; Slowing, I. I.; Sadow, A. D.; Pruski, M. Dynamic Nuclear Polarization Solid-State NMR in Heterogeneous Catalysis Research. *ACS Catal.* **2015**, *5* (12), 7055–7062.
- (57) Lummiss, J. A. M.; Perras, F. A.; McDonald, R.; Bryce, D. L.; Fogg, D. E. Sterically Driven Olefin Metathesis: The Impact of Alkylidene Substitution on Catalyst Activity. *Organometallics* **2016**, *35* (5), 691–698.
- (58) Gordon, C. P.; Copéret, C. Chemical Shift Tensors - Why Should We Care? *Chimia* **2019**, *73* (4), 252–256.
- (59) Gordon, C. P.; Yamamoto, K.; Searles, K.; Shirase, S.; Andersen, R. A.; Eisenstein, O.; Copéret, C. Metal alkyls programmed to generate metal alkylidenes by α -H abstraction: prognosis from NMR chemical shift. *Chem. Sci.* **2018**, *9* (7), 1912–1918.
- (60) Gordon, C. P.; Shirase, S.; Yamamoto, K.; Andersen, R. A.; Eisenstein, O.; Copéret, C. NMR chemical shift analysis decodes olefin oligo- and polymerization activity of dgroup 4 metal complexes. *Proc. Natl. Acad. Sci. U. S. A.* **2018**, *115* (26), ES867–ES876.
- (61) Ramsey, N. F. Magnetic Shielding of Nuclei in Molecules. *Phys. Rev.* **1950**, *78* (6), 699–703.
- (62) Liu, S. F.; Mao, J. D.; Schmidt-Rohr, K. A Robust Technique for Two-Dimensional Separation of Undistorted Chemical-Shift Anisotropy Powder Patterns in Magic-Angle-Spinning NMR. *J. Magn. Reson.* **2002**, *155* (1), 15–28.
- (63) Culver, D. B.; Huynh, W.; Tafazolian, H.; Ong, T.-C.; Conley, M. P. The β -Agostic Structure in (C₅Me₅)₂Sc(CH₂CH₃): Solid-State NMR Studies of (C₅Me₅)₂Sc-R (R = Me, Ph, Et). *Angew. Chem., Int. Ed.* **2018**, *57* (30), 9520–9523.
- (64) Zhao, Y.; Truhlar, D. G. A new local density functional for main-group thermochemistry, transition metal bonding, thermochemical kinetics, and noncovalent interactions. *J. Chem. Phys.* **2006**, *125* (19), 194101–194119.
- (65) Weigend, F. Accurate Coulomb-fitting basis sets for H to Rn. *Phys. Chem. Chem. Phys.* **2006**, *8* (9), 1057–1065.
- (66) Weigend, F.; Ahlrichs, R. Balanced basis sets of split valence, triple zeta valence and quadruple zeta valence quality for H to Rn: Design and assessment of accuracy. *Phys. Chem. Chem. Phys.* **2005**, *7* (18), 3297–3305.
- (67) Frisch, M. J.; Trucks, G. W.; Schlegel, H. B.; Scuseria, G. E.; Robb, M. A.; Cheeseman, J. R.; Scalmani, G.; Barone, V.; Mennucci, B.; Petersson, G. A.; Nakatsuji, H.; Caricato, M.; Li, X.; Hratchian, H. P.; Izmaylov, A. F.; Bloino, J.; Zheng, G.; Sonnenberg, J. L.; Hada, M.; Ehara, M.; Toyota, K.; Fukuda, R.; Hasegawa, J.; Ishida, M.; Nakajima, T.; Honda, Y.; Kitao, O.; Nakai, H.; Vreven, T.; Montgomery, J. A., Jr.; Peralta, J. E.; Ogliaro, F.; Bearpark, M.; Heyd, J. J.; Brothers, E.; Kudin, K. N.; Staroverov, V. N.; Kobayashi, R.; Normand, J.; Raghavachari, K.; Rendell, A.; Burant, J. C.; Iyengar, S. S.; Tomasi, J.; Cossi, M.; Rega, N.; Millam, J. M.; Klene, M.; Knox, J. E.; Cross, J. B.; Bakken, V.; Adamo,

C.; Jaramillo, J.; Gomperts, R.; Stratmann, R. E.; Yazyev, O.; Austin, A. J.; Cammi, R.; Pomelli, C.; Ochterski, J. W.; Martin, R. L.; Morokuma, K.; Zakrzewski, V. G.; Voth, G. A.; Salvador, P.; Dannenberg, J. J.; Dapprich, S.; Daniels, A. D.; Farkas, O.; Foresman, J. B.; Ortiz, J. V.; Cioslowski, J.; Fox, D. J. *Gaussian 09*, revision E.01; Gaussian, Inc.: Wallingford, CT, 2009.

(68) Littrell, J. C.; Talley, C. E.; Dallinger, R. F.; Gilbert, T. M. Raman Spectra of $M_2(OR)_6$ and M_2R_6 ($M = Mo, W$) Compounds: Assignment of the M:M Stretching Frequency in M_2X_6 Dimers. *Inorg. Chem.* **1997**, *36* (5), 760–761.

(69) Mazoyer, E.; Merle, N.; Mallmann, A. d.; Basset, J. M.; Berrier, E.; Delevoye, L.; Paul, J. F.; Nicholas, C. P.; Gauvin, R. M.; Taoufik, M. Development of the First Well-Defined Tungsten Oxo Alkyl Derivatives Supported on Silica by SOMC: Towards a Model of WO_3/SiO_2 Olefin Metathesis Catalyst. *Chem. Commun.* **2010**, *46*, 8944–8946.

(70) Grekov, D.; Bouhoute, Y.; Szeto, K. C.; Merle, N.; De Mallmann, A.; Lefebvre, F.; Lucas, C.; Del Rosal, I.; Maron, L.; Gauvin, R. M.; Delevoye, L.; Taoufik, M. Silica-Supported Tungsten Neosilyl Oxo Precatalysts: Impact of the Podality on Activity and Stability in Olefin Metathesis. *Organometallics* **2016**, *35* (13), 2188–2196.

(71) Rhers, B.; Salameh, A.; Baudouin, A.; Quadrelli, E. A.; Taoufik, M.; Copéret, C.; Lefebvre, F.; Basset, J.-M.; Solans-Monfort, X.; Eisenstein, O.; Lukens, W. W.; Lopez, L. P. H.; Sinha, A.; Schrock, R. R. A Well-Defined, Silica-Supported Tungsten Imido Alkylidene Olefin Metathesis Catalyst. *Organometallics* **2006**, *25* (15), 3554–3557.

(72) Syed, Z. H.; Kaphan, D. M.; Perras, F. A.; Pruski, M.; Ferrandon, M. S.; Wegener, E. C.; Celik, G.; Wen, J.; Liu, C.; Dogan, F.; Goldberg, K. I.; Delferro, M. Electrophilic Organoiridium(III) Pincer Complexes on Sulfated Zirconia for Hydrocarbon Activation and Functionalization. *J. Am. Chem. Soc.* **2019**, *141* (15), 6325–6337.

(73) Liu, S.; Tan, J. M.; Gulec, A.; Schweitzer, N. M.; Delferro, M.; Marks, L. D.; Stair, P. C.; Marks, T. J. Direct Synthesis of Low-Coordinate Pd Catalysts Supported on SiO_2 via Surface Organometallic Chemistry. *ACS Catal.* **2016**, *6* (12), 8380–8388.

(74) Jeantelot, G.; Qureshi, M.; Harb, M.; Ould-Chikh, S.; Anjum, D. H.; Abou-Hamad, E.; Aguilar-Tapia, A.; Hazemann, J.-L.; Takanabe, K.; Basset, J.-M. TiO_2 -supported Pt single atoms by surface organometallic chemistry for photocatalytic hydrogen evolution. *Phys. Chem. Chem. Phys.* **2019**, *21*, 24429–24440.

(75) Yang, D.; Xu, P.; Browning, N. D.; Gates, B. C. Tracking Rh Atoms in Zeolite HY: First Steps of Metal Cluster Formation and Influence of Metal Nuclearity on Catalysis of Ethylene Hydrogenation and Ethylene Dimerization. *J. Phys. Chem. Lett.* **2016**, *7* (13), 2537–2543.

(76) In addition to the lack of activity of the supernatant solution after the reaction suggesting that the active species is not leached off of the silica surface, the filtered and recycled catalyst showed similar activity in the related self-metathesis of 1-octene to generate ethylene and *cis*- and *trans*-tetradecene.

(77) Genelot, M.; Cheval, N. P.; Vitorino, M.; Berrier, E.; Weibel, J. M.; Pale, P.; Mortreux, A.; Gauvin, R. M. Well-Defined Silica-Supported Molybdenum Nitride Species: Silica Grafting Triggers Alkyne Metathesis Activity. *Chem. Sci.* **2013**, *4*, 2680–2685.

(78) Zhizhko, P. A.; Zhizhin, A. A.; Zarubin, D. N.; Ustynyuk, N. A. Oxo/Imido Heterometathesis between N-Sulfinylamines and Ketones Catalyzed by a Silica-Supported Molybdenum Imido Complex. *Mendeleev Commun.* **2012**, *22*, 64–66.

(79) Gajan, D.; Rendon, N.; Wampler, K. M.; Basset, J.-M.; Coperet, C.; Lesage, A.; Emsley, L.; Schrock, R. R. Synthesis and Reactivity of Molybdenum Imido Alkylidene Bis-Pyrazolide Complexes. *Dalton Trans.* **2010**, *39*, 8547–8551.

(80) An additional potential deactivation pathway for the alkyl dimers may be through the nucleophilicity of the neopentylidene species which may then form inactive alkylidene-bridged intermediates.